Technical and Clinical Factors Affecting Success Rate of a Deep Learning Method for Pancreas Segmentation on CT

Mohammad Hadi Bagheri, MD, Holger Roth, PhD, William Kovacs, BS, Jianhua Yao, PhD, Faraz Farhadi, BS, Xiaobai Li, PhD, Ronald M. Summers, MD, PhD**

Abbreviations

DSC
Dice similarity coefficient

BMI
body mass index

CNN
convolutional neural network

HNN
holistically-nested neural networks

DFOV
Display Field of View

Purpose: Accurate pancreas segmentation has application in surgical planning, assessment of diabetes, and detection and analysis of pancreatic tumors. Factors that affect pancreas segmentation accuracy have not been previously reported. The purpose of this study is to identify technical and clinical factors that adversely affect the accuracy of pancreas segmentation on CT.

Method and Materials: In this IRB and HIPAA compliant study, a deep convolutional neural network was used for pancreas segmentation in a publicly available archive of 82 portal-venous phase abdominal CT scans of 53 men and 29 women. The accuracies of the segmentations were evaluated by the Dice similarity coefficient (DSC). The DSC was then correlated with demographic and clinical data (age, gender, height, weight, body mass index), CT technical factors (image pixel size, slice thickness, presence or absence of oral contrast), and CT imaging findings (volume and attenuation of pancreas, visceral abdominal fat, and CT attenuation of the structures within a 5 mm neighborhood of the pancreas).

Results: The average DSC was 78% $\pm$ 8%. Factors that were statistically significantly correlated with DSC included body mass index ($r = 0.34$, $p < 0.01$), visceral abdominal fat ($r = 0.51$, $p < 0.0001$), volume of the pancreas ($r = 0.41$, $p = 0.001$), standard deviation of CT attenuation within the pancreas ($r = 0.30$, $p = 0.01$), and median and average CT attenuation in the immediate neighborhood of the pancreas ($r = -0.53$, $p < 0.0001$ and $r = -0.52$, $p < 0.0001$). There were no significant correlations between the DSC and the height, gender, or mean CT attenuation of the pancreas.

Conclusion: Increased visceral abdominal fat and accumulation of fat within or around the pancreas are major factors associated with more accurate segmentation of the pancreas. Potential applications of our findings include assessment of pancreas segmentation difficulty of a particular scan or dataset and identification of methods that work better for more challenging pancreas segmentations.

Key Words: Pancreas; Segmentation; Deep Learning; Computed Tomography.

Acad Radiol 2020; 27:689–695

From the Clinical Image Processing Service, Radiology and Imaging Sciences Department, Clinical Center, National Institutes of Health, Bethesda, MD 20892-1182, USA (M.H.B., W.K., J.Y.); Imaging Biomarkers and Computer-aided Diagnosis Laboratory, Radiology and Imaging Sciences Department, Clinical Center, National Institutes of Health, Building 10 Room 1C224D MSC 1182, Bethesda, MD 20892-1182 (H.R., R.M.S.); Radiology and Imaging Sciences, National Institutes of Health Clinical Center, Bethesda, MD (F.F.); Biostatistics and Clinical Epidemiology Service (BCES), National Institutes of Health Clinical Center, Bethesda, MD (X.L.). Received July 23, 2019; revised August 21, 2019; accepted August 27, 2019. Funding: This work was supported by the Intramural Research Program of the NIH Clinical Center 1Z01 CL040004. Presented at the 2016 RSNA Annual Meeting, Chicago Illinois November 26–December 3, 2016. **Address correspondence to:** R.M.S. e-mail: rms@nih.gov
** https://www.cc.nih.gov/drd/summers.html

https://doi.org/10.1016/j.acra.2019.08.014

INTRODUCTION

Pancreas segmentation has application in surgical planning, assessment of diabetes and detection, and analysis of pancreatic adenocarcinoma and neuroendocrine tumors (1,2). The pancreas is a small flexible soft tissue intra-abdominal organ, which is highly variable and complex in shape, size, and CT attenuation from patient to patient. In addition, the CT attenuation of the pancreas can be similar to that of adjacent structures such as bowel and blood vessels depending on the presence and timing of administration of oral and intravenous contrast. As such, accurate segmentation of the pancreas on CT scans is a challenging problem compared to that of larger more rigid organs such as the liver, spleen, and kidneys.

Recent investigation has centered on applying deep convolutional neural networks (deep CNNs) for organ segmentation. Deep CNNs are a type of machine learning that performs automatic multi-level feature extraction from training images while simultaneously learning classification or regression tasks (3). Deep learning has been shown to be very useful for localization and segmentation in many difficult medical imaging tasks (4,5). Performance of deep learning for organ segmentation depends not only on the details of the deep learning method but also on the complexity of the organ and its neighboring anatomic structures. Therefore, organ segmentation performance is highly task dependent. This is exemplified by the considerable variation in published success rate with pancreas segmentation accuracy and by the lower accuracies compared to the other organs (6–21). At present, we have little information about the reasons for this reduced and variable performance in different patients and datasets. Such information could help guide future research to improve performance.

We utilized a specialized group of deep CNNs called holistically-nested neural networks (HNN) which has comparable multi-scale convolutional structure and performance to the U-Nets used by other investigators (22). In this study, we compared the success rate of this Deep CNN method for automated pancreas segmentation with a multiplicity of technical, demographic, and clinical factors.

METHOD AND MATERIALS

This study was IRB-approved and HIPAA compliant.

Dataset

The dataset consisted of abdominal CT scans in 82 patients (53 men and 29 women) from a publicly available archive (23,24). The patients' mean age was 46.8 ± 16.7 (Range = 18–76). Seventeen patients were healthy kidney donors. The remaining 65 patients had neither major abdominal pathologies nor pancreatic lesions. All scans were obtained in the portal-venous phase (~70 seconds after intravenous contrast injection) on Philips and Siemens multidetector CT scanners (120 kVp tube voltage). Mean slice thickness was 1.2 ± 0.7 mm. The pixel size was 0.851 × 0.851 ±0.09 mm.

Reference standard segmentations were manual slice-by-slice tracings of the pancreases by a medical student. This reference standard was verified and corrected if needed by an experienced radiologist.

Segmentation

A modified holistic deep convolutional neural network was used (7,22). The method uses a coarse-to-fine approach common to other recent pancreas segmentation research (11,12,25,26). Briefly, the method consists of several steps (more details are found in (7,23,27)).

The first step crops the CT scan to the region containing the pancreas. First, a superpixel method with random forest classifier was used to get a 3D bounding box of the pancreas with high recall. The method removes large background (i.e. nonpancreas) regions in the CT scan, but retains candidate pancreas regions. Next, the method selects a 3D bounding box around the retained superpixels to crop to the pancreas region. This step detected all pancreas regions with 100% recall while removing most of the background.

The second step performs a detailed segmentation of the pancreas. Two HNN models are trained to generate interior (HNN-I) and boundary (HNN-B) maps of the pancreas. The two maps allow the deep learning models to learn complementary features of the pancreas interior and its boundary region in order to improve the overall segmentation accuracy of the system. The two maps are then fused by a random forest classifier based on superpixel analysis (1). The result is a high-resolution segmentation of the pancreas.

We produced segmentation results for our dataset based on a 4-fold split where in each fold 75% and 25% of patients were used for training and inference, respectively.

Assessment

The segmentation was evaluated using the Dice similarity coefficient (DSC):

$$\mathrm{DSC} = \frac{2|P \cap G|}{|P| + |G|}$$

Here, $|P|$ and $|G|$ are the number of predicted pancreas voxels and the ground truth voxels belonging to the pancreas region in the CT image, respectively. $|P \cap G|$ denotes the number of voxels where both predicted and ground truth pancreas regions overlap. The DSC of each pancreas segmentation was computed on a per-patient basis and was correlated to the CT technical factors (image pixel size, slice thickness, and presence or absence of oral contrast), demographic data (age, gender, height, weight, body mass index [BMI]), and the CT imaging findings (volume and attenuation of pancreas, visceral abdominal fat volume, subcutaneous abdominal fat volume, and CT attenuation of the soft tissues within a 5-mm neighborhood of the pancreas). The visceral and subcutaneous abdominal fat volumes were measured through an inhouse automated algorithm consisting of five steps: body masking, noise reduction, adipose tissue labeling, visceral and subcutaneous adipose tissue separation, and volume quantification (28,29). The CT imaging findings of the pancreas and its neighborhood were computed from the manual segmentation reference standard.

Statistical Analysis

To assess the relationships between the segmentation performance and the clinical and technical factors, Spearman correlation analysis of the DSC was performed (SAS, Version 14.2 and Microsoft Excel Version 16). Significance was defined as

a difference with $p < 0.05$. The distributions of the factors such as age and abdominal fat were evaluated by histogram and Shapiro-Wilk test. Welch Two Sample *t* test was used to compare DSC in men and women and in presence or absence of oral contrast. The correlation analysis was visualized using a heat map (R Statistical Software, R Studio: Integrated Development Environment for R, version 1.2.1335, Boston, MA). One-way ANOVA of DSC versus gender and oral contrast presence was also calculated using R.

RESULTS

The average DSC of the pancreas segmentations was 78% ± 8%. Of the demographic and clinical factors, BMI showed positive significant correlation with DSC (Table 1 and Fig 1). Age showed a mild positive correlation that reached borderline significance. There was a normal distribution of the cases by age. There was no significant correlation with height. There was no significant difference between the DSC values in men and women ($p = 0.3$, 95% CI = [-0.06, 0.02]) (Table 1 and Fig 1).

For the CT technical factors, no significant statistical correlation was found between the DSC and slice thickness or the presence or absence of oral contrast material in the bowel. A positive correlation was noted between DSC and image pixel size (Table 1 and Fig 1).

The CT findings encompass 3 parts: body fat, pancreas parenchyma, and pancreas neighborhood. Among the body fat factors, those having a statistically significant correlation with DSC were visceral abdominal fat and total abdominal fat (Fig 1). The distribution histogram of visceral abdominal fat showed slightly more cases with low abdominal fat, assuring that these cases were not underrepresented (skewness = +0.69). For the pancreas parenchymal factors, the volume of the pancreas and standard deviation of CT attenuation within the pancreas showed significant correlation (Fig 1). No positive correlation was found between the DSC and mean and median CT attenuation of the pancreas. The pancreas neighborhood factors having significant correlation were median and average CT attenuation (Figs 2–4). There was a strong negative correlation with the average and median CT attenuation of the neighborhood of the pancreas. There were no significant correlations with standard deviation, minimum, and maximum attenuation of the pancreas neighborhood.

DISCUSSION

In this study, we found that factors that were statistically significantly correlated with DSC included BMI, visceral abdominal fat, volume of the pancreas, and median and average CT attenuation in the immediate neighborhood of the pancreas. These correlations make sense, because a pancreas that is better delineated by fat will be easier to segment from adjacent structures like bowel and other organs. Larger pancreases are also easier to segment with higher DSCs, since small segmentation errors cause a smaller decrease in DSC for larger organs compared to smaller ones.

No correlation was noted between segmentation accuracy and average CT attenuation of the pancreas. This suggests that contrast enhancement variation due to contrast bolus timing or cardiac output were less important factors.

TABLE 1. Correlation of the Clinical and CT Imaging Factors with DSC of Deep Learning Method for Automated Pancreas Segmentation

Type	Factors	Avg (Range)	*r*	*p*
Demographic and clinical	Age (y)	46.6 (18, 76)	0.22	0.050
	Sex*	NA	NA	0.304
	Height (cm)	171.3 (148.8, 195.4)	−0.19	0.095
	Weight (kg)	79.8 (43.0, 128.4)	0.21	0.061
	BMI (kg/m^2)	27 (17, 40)	0.34	0.002
CT technical factors	Image pixel size X (mm)	0.85 (0.66, 0.97)	0.31	0.004
	Image pixel size Y (mm)	0.85 (0.66, 0.97)	0.31	0.004
	Slice thickness (pixel size Z)	1.15 (0.49, 5.0)	−0.16	0.150
	Presence or absence of iodine oral contrast in the bowel*	NA	NA	0.709
CT findings - pancreas	Volume (cm^3)	73.5 (42.3, 150.0)	0.41	<0.001
	Average attenuation (HU)	86.7 (37.1, 127.0)	−0.18	0.100
	Median attenuation (HU)	90.2 (44, 133)	−0.17	0.127
	Standard Deviation (HU)	32.2 (17.5, 64.7)	0.37	<0.001
CT findings – pancreas 5 mm neighborhood	Median attenuation (HU)	35.5 (−75.0, 124.0)	−0.53	<0.001
	Average attenuation (HU)	36.7 (−44.2, 127.5)	−0.52	<0.001
CT Findings – abdominal fat volume/body volume	Visceral fat	0.11 (0.02, 0.29)	0.51	<0.001
	Subcutaneous fat	0.22 (0.05, 0.55)	0.20	0.074
	Total fat	0.33 (0.05, 0.29)	0.36	<0.001

r = Spearman correlation; *p* = *p* value; HU = Hounsfield Units.

* Statistical analysis using One-way Anova.

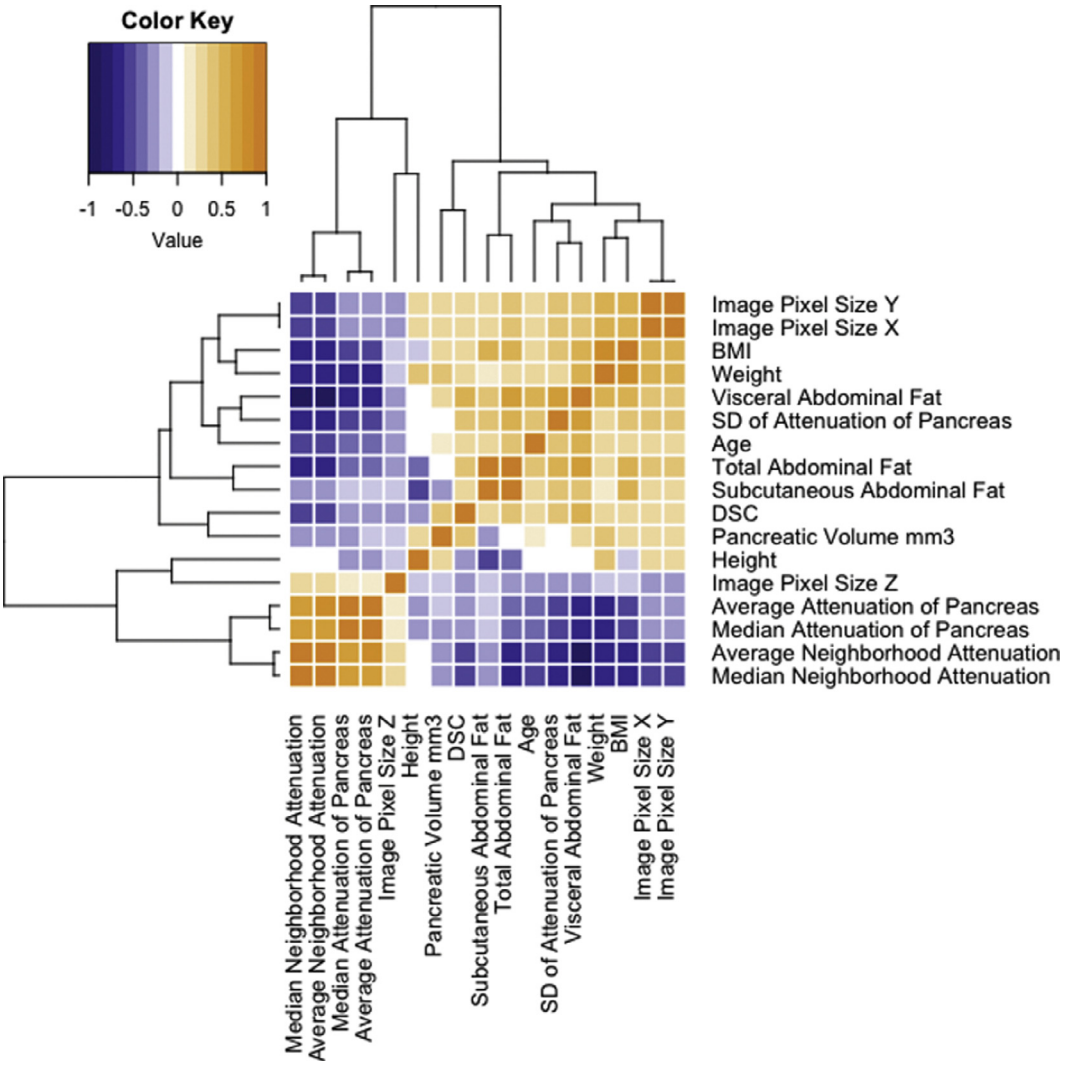

Figure 1. Heat map for correlation (Spearman *r*) of different factors and the performance of deep learning. The strongest positive correlation is between DSC and visceral abdominal fat and the strongest negative correlation of DSC was with average and median neighborhood attenuation of pancreas. Dendrogram shows the similarity or distance between rows or columns. The heat map shows similarity or association between visceral abdominal fat and standard deviation of CT density of the pancreas. Both have some similarity with age. All have some correlation with BMI and weight. Image pixel size z = slice thickness. (Color version of figure is available online.)

However, the standard deviation of the CT attenuation of the pancreas did show significant positive correlation with the DSC. With aging or diabetes, for example, there will be more fat deposition inside the pancreas itself. This will cause higher standard deviation of the CT attenuation of the pancreas. A possible explanation for the positive correlation is that more uniform pancreas attenuation textures make it more difficult for the deep learning algorithm to separate pancreas from adjacent structures. In contrast, pancreases with increased texture due to internal fat deposition may present a more characteristic pattern that distinguishes the pancreas from adjacent structures which do not have similar patterns.

We found a positive correlation between DSC and the pixel size. This can be explained by the fact that with a larger abdomen secondary to obesity, the Display Field of View must be large enough to cover the whole abdomen in the axial image leading to larger pixels with higher signal to noise ratios. So, better performance with larger pixel size might be related to more fat deposition in the abdomen rather than the pixel size itself. On the other hand, smaller pixel sizes may be associated with more noise which could make segmentation more difficult.

We used a deep learning pancreas segmentation method that performed comparably to others in the literature based on its DSC. The patient population was a reasonably diverse one, spanning a wide spectrum of ages that was normally distributed.

Organ detection, segmentation, and boundary refinement on radiology studies such as CT scans are very important for lesion detection, disease diagnosis, and quantitative measurements of the organs. When automated, organ segmentation can enhance lesion detection and facilitate diagnosis and treatment (30–32).

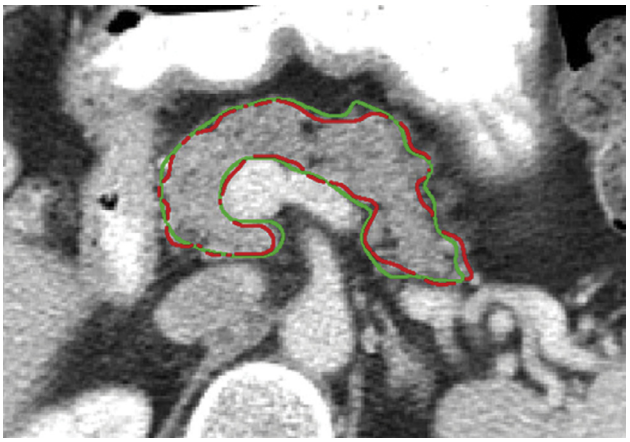

Figure 2. Comparison of automated pancreas segmentation (red) with manual tracing (green) on CT of a 62-year-old woman. The pancreas is relatively well-delineated by peripancreatic fat. There is mild to moderate heterogeneity of intrapancreatic CT attenuation due to islands of fat. DSC = 0.81. Standard deviation of pancreatic attenuation = 49.7 HU. Average attenuation of pancreatic neighborhood = 21.7 HU. (Color version of figure is available online.)

CT of the abdomen is one of the most commonly used imaging studies for evaluation of abdominal structures. Multidetector CT is the modality of choice for diagnosis and follow-up of pancreatic tumors (33–35). More widely available automated measurements of the pancreas might expand applications in diabetes.

Pancreas segmentation on CT is challenging even for experienced radiologists. This is mainly due to variations in shape and morphology of the pancreas, close similarity of its attenuation to that of the nearby structures, and crowded anatomy in the upper abdomen with many closely abutting structures (36). As such, the accuracy of automated pancreas segmentation is much less than that for other abdominal organs such as the liver, spleen, and kidneys (30,37–39). In a

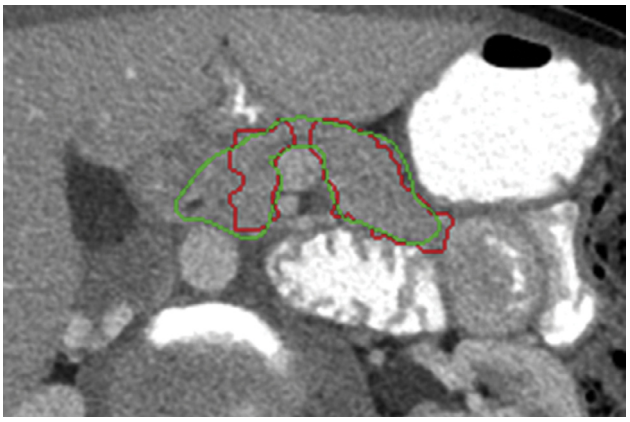

Figure 3. Automated pancreas segmentation (red) with manual tracing (green) of the pancreas in a 48-year-old woman. The pancreas is poorly delineated due to an absence of peripancreatic fat. There is relatively homogeneous intrapancreatic CT attenuation. DSC = 0.61. Standard Deviation of pancreatic attenuation = 17.5 HU. Average Attenuation of Pancreatic Neighborhood = 108.2 HU. (Color version of figure is available online.)

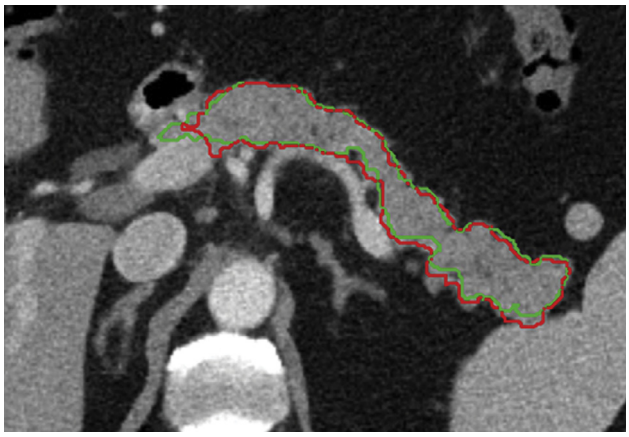

Figure 4. Automated (red) and manual tracing (green) of pancreas in a 52-year-old man. The pancreas is well-delineated by abundant peripancreatic fat. There is mild heterogeneity of intrapancreatic CT attenuation. DSC = 0.84. Standard Deviation of pancreatic attenuation = 33.1 HU. Average Attenuation of Pancreatic Neighborhood = −35.1 HU. (Color version of figure is available online.)

similar context, pulmonary nodules attached to the pleura and mediastinum are difficult to detect and segment automatically as the attenuation of the nodule is similar to that of the adjacent chest wall or mediastinum (40).

Intra- and interobserver variability are known problems for clinical use of manual segmentations of organs and tumors. For example, one study found mean volume overlap variability values of 8.8% for kidney outline delineation by two observers (41). Automated segmentations would be expected to reduce or eliminate such variability.

It is important to know what clinical and technical factors can affect the performance of organ segmentation and in particular pancreas segmentation. Quality of the CT scan and technical factors can play a major role in organ and lesion segmentation. For example, various acquisition parameters can affect the performance of lesion volumetry on hepatic CT scans (42). Factors such as the CT scanner type and generation, volume and concentration of the iodinated contrast injected, the rate of injection, patient age, weight and cardiac output all play a role in maximal pancreatic enhancement for better detection of lesions in the pancreas (35). Nevertheless, we found no relevant publication to date regarding the effect of clinical and demographic factors on the performance of automated segmentation of the pancreas.

Segmentation studies in the literature sometimes use publicly available datasets and sometimes do not. When studies use non-public datasets, case difficulty is an open question that inhibits the scientific community's ability to compare segmentation results from one publication to another. This study provides important metrics that could be used to compare difficulty of pancreas segmentation datasets. Similar metrics have been reportedly found useful for other radiologic tasks, for example colon preparation quality on CT colonography (43,44).

These findings are the same for human perception. A radiologist can better differentiate the pancreas from adjacent structures when there is more fat surrounding the pancreas

(45) and more heterogeneous texture of it secondary to fat deposition. Our findings shed more light on the performance of deep learning methods and its similarity to the radiologist's image perception.

This study has several limitations. We used only the portal venous phase of the abdominal CT scans. Multiphasic pancreas imaging including arterial and parenchymal phases may increase the accuracy of the segmentation. However, arterial phase images are mainly of value for detecting hypervascular tumors in the pancreas. Also, portal venous phase images are expected to have greater image contrast between the pancreas, adjacent fat, and splenic vein than arterial phase images thereby permitting more accurate pancreas segmentations. The total number of cases was relatively limited and all pancreases were normal. Further studies with larger sample sizes and with abnormal pancreases can yield more information regarding the performance of deep learning in pancreas segmentation in different clinical and technical settings. Larger sample sizes may also improve training of the deep learning algorithm leading to higher overall DSC. The same factors that affect the results for the normal pancreases would be expected to also apply to abnormal pancreases, although the type and severity of the abnormality will also be important. This study used only a single deep learning method to segment the pancreas. Although our segmentation method had high performance, other published high-performing pancreas segmentation methods may exhibit different correlations with patient characteristics. The manual segmentations were done by a single observer supervised by a radiologist. Inter- and intraobserver variability of the manual segmentations could also lead to different correlations with patient characteristics because the DSCs would change.

In conclusion, increased visceral abdominal fat, and deposition of fat within or around the pancreas are major factors associated with better segmentation of the pancreas. The inclusion of more training examples of CT from patients with lesser amounts of such fat may improve overall pancreas segmentation accuracy.

DISCLOSURES

M.H.B: Nothing to disclose.
H.R: Employee of NVIDIA
W.K: Nothing to disclose.
J.Y: Patent royalties from iCAD, Employee of TenCent
F.F: Nothing to disclose.
X.L: Nothing to disclose.
R.M.S: Royalties from iCAD, ScanMed, Philips & Ping An. Research support from Ping An and NVIDIA.

ACKNOWLEDGMENTS

We thank Francine Thomas for collecting clinical data, Uyen N. Hoang for assistance in statistical analysis and Drs. Nathan Lay and Youbao Tang for assistance with figure preparation.

REFERENCES

1. Chu LC, Park S, Kawamoto S, et al. Utility of CT radiomics features in differentiation of pancreatic ductal adenocarcinoma from normal pancreatic tissue. AJR Am J Roentgenol 2019: 1–9.
2. Okamoto T, Onda S, Yasuda J, et al. Navigation surgery using an augmented reality for pancreatectomy. Dig Surg 2015; 32:117–123.
3. LeCun Y, Bengio Y, Hinton G. Deep learning. Nature 2015; 521:436–444.
4. Litjens G, Kooi T, Bejnordi BE, et al. A survey on deep learning in medical image analysis. Med Image Anal 2017; 42:60–88.
5. Sahiner B, Pezeshk A, Hadjiiski LM, et al. Deep learning in medical imaging and radiation therapy. Med Phys 2019; 46:e1–e36.
6. Farag A, Lu L, Turkbey E, et al. A bottom-up approach for automatic pancreas segmentation in abdominal CT scans. In: Yoshida H, Näppi JJ, Saini S, eds. Abdominal imaging computational and clinical applications: 6th International Workshop, ABDI 2014, Held in Conjunction with MICCAI 2014, Cambridge, MA, USA, September 14, 2014, Cham. Springer International Publishing; 2014:103–113.
7. Roth HR, Lu L, Lay N, et al. Spatial aggregation of holistically-nested convolutional neural networks for automated pancreas localization and segmentation. Med Image Anal 2018; 45:94–107.
8. Roth H, Oda M, Shimizu N, et al. Towards dense volumetric pancreas segmentation in CT using 3D fully convolutional networks. SPIE Med Imaging 2018; 6. doi:10.1117/12.2293499.
9. Zhou Y, Xie L, Shen W, et al. A fixed-point model for pancreas segmentation in abdominal CT scans. Cham: Springer International Publishing, 2017:693–701.
10. Karasawa K, Oda M, Kitasaka T, et al. Multi-atlas pancreas segmentation: atlas selection based on vessel structure. Med Image Anal 2017; 39:18–28.
11. Zhu ZT, Xia YD, Shen W, et al. A 3D coarse-to-fine framework for volumetric medical image segmentation. In: Int Conf 3d Vision; 2018. p. 682–690.
12. Yu QH, Xie LX, Wang Y, et al. Recurrent saliency transformation network: incorporating multi-stage visual cues for small organ segmentation. In: 2018 IEEE/CVF Conference on Computer Vision and Pattern Recognition (CVPR); 2018. p. 8280–8289.
13. Zhou XR, Takayama R, Wang S, et al. Automated segmentation of 3D anatomical structures on CT images by using a deep convolutional network based on end-to-end learning approach. In: Medical imaging 2017: image processing; 2017. p. 10133.
14. Fu M, Wu WM, Hong XF, et al. Hierarchical combinatorial deep learning architecture for pancreas segmentation of medical computed tomography cancer images. Bmc Syst Biol 2018; 12:56.
15. Gibson E, Giganti F, Hu Yp, et al. Automatic multi-organ segmentation on abdominal CT with dense V-networks. IEEE Trans Med Imaging 2018; 37:1822–1834.
16. Heinrich MP, Blendowski M, Oktay O. TernaryNet: faster deep model inference without GPUs for medical 3D segmentation using sparse and binary convolutions. Int J Comput Assist Radiol Surg 2018; 13:1311–1320.
17. Man Y, Huang Y, Li JFX, et al. Deep Q learning driven CT Pancreas Segmentation with Geometry-Aware U-Net. IEEE Trans Med Imaging 2019.
18. Asaturyan H, Gligorievski A, Villarini B. Morphological and multi-level geometrical descriptor analysis in CT and MRI volumes for automatic pancreas segmentation. Comput Med Imaging Graph 2019; 75:1–13.
19. Roth HR, Oda H, Zhou X, et al. An application of cascaded 3D fully convolutional networks for medical image segmentation. Comput Med Imaging Graph 2018; 66:90–99.
20. Okada T, Linguraru MG, Hori M, et al. Abdominal multi-organ segmentation from CT images using conditional shape-location and unsupervised intensity priors. Med Image Anal 2015; 26:1–18.
21. Tong T, Wolz R, Wang Z, et al. Discriminative dictionary learning for abdominal multi-organ segmentation. Med Image Anal 2015; 23:92–104.
22. Xie S, Tu Z. Holistically-nested edge detection. In: ICCV; 2015. p. 1395–1403.
23. Roth HR, Lu L, Farag A, et al. DeepOrgan: multi-level deep convolutional networks for automated pancreas segmentation. In: MICCAI 2015, Part I, LNCS, 2015; 9349. p. 556–564.
24. Roth H, Farag A, Turkbey E, Lu L, Liu J, Summers RM. Data from pancreas-CT. The cancer imaging archive. Available at: http://dx.doi.org/10.7937/K9/TCIA.2016.tNB1kqBU. Accessed June 28, 2019.
25. Zhou Y, Xie L, Shen W, et al. Pancreas segmentation in abdominal CT scan: a coarse-to-fine approach. arXiv preprint arXiv:161208230. 2016.
26. Zhu Z, Xia Y, Shen W, et al. A 3D coarse-to-fine framework for automatic pancreas segmentation. arXiv preprint arXiv:171200201. 2017.

27. Roth HR, Lu L, Farag A, et al. Spatial aggregation of holistically-nested networks for automated pancreas segmentation. In: MICCAI 2016, Part II, LNCS, 2016; 9901. p. 451–459.
28. Summers RM, Liu J, Sussman DL, et al. Association between visceral adiposity and colorectal polyps on CT colonography. AJR Am J Roentgenol 2012; 199:48–57.
29. Liu J, Pattanaik S, Yao J, et al. Associations among pericolonic fat, visceral fat, and colorectal polyps on CT colonography. Obesity (Silver Spring) 2015; 23:408–414.
30. Tong T, Wolz R, Wang Z, et al. Discriminative dictionary learning for abdominal multi-organ segmentation. Med Image Anal 2015; 23:92–104.
31. Cerrolaza JJ, Villanueva A, Reyes M, et al. Generalized multiresolution hierarchical shape models via automatic landmark clusterization. In: Golland P, Hata N, Barillot C, Hornegger J, Howe R, eds. Medical image computing and computer-assisted intervention – MICCAI 2014: 17th international conference, Boston, MA, USA, September 14-18, 2014, proceedings, Part III, Cham. Springer International Publishing; 2014:1–8.
32. Okada T, Linguraru MG, Hori M, et al. Abdominal multi-organ segmentation from CT images using conditional shape–location and unsupervised intensity priors. Med Image Anal 2015; 26:1–18.
33. Granata V, Fusco R, Catalano O, et al. Multidetector computer tomography in the pancreatic adenocarcinoma assessment: an update. Infect Agents Cancer 2016; 11:57.
34. Lee ES, Lee JM. Imaging diagnosis of pancreatic cancer: a state-of-the-art review. World J Gastroenterol 2014; 20:7864–7877.
35. Brennan DD, Zamboni GA, Raptopoulos VD, et al. Comprehensive preoperative assessment of pancreatic adenocarcinoma with 64-section volumetric CT. Radiographics 2007; 27:1653–1666.
36. Hammon M, Cavallaro A, Erdt M, et al. Model-based pancreas segmentation in portal venous phase contrast-enhanced CT images. J Digit Imaging 2013; 26:1082–1090.
37. Chu C, Oda M, Kitasaka T, et al. Multi-organ segmentation based on spatially-divided probabilistic atlas from 3D abdominal CT images. In: Mori K, Sakuma I, Sato Y, Barillot C, Navab N, eds. Medical image computing and computer-assisted intervention – MICCAI 2013: 16th international conference, Nagoya, Japan, September 22-26, 2013, Proceedings, Part II, Berlin, Heidelberg. Springer Berlin Heidelberg; 2013:165–172.
38. Oda M, Nakaoka T, Kitasaka T, et al. Organ segmentation from 3D abdominal CT images based on atlas selection and graph cut. In: Yoshida H, Sakas G, Linguraru MG, eds. Abdominal imaging computational and clinical applications: third international workshop, held in conjunction with MICCAI 2011, Toronto, ON, Canada, September 18, 2011, revised selected papers, Berlin, Heidelberg. Springer Berlin Heidelberg; 2012:181–188.
39. Karasawa Ki, Kitasaka T, Oda M, et al. Structure specific atlas generation and its application to pancreas segmentation from contrasted abdominal CT volumes. In: Menze B, Langs G, Montillo A, eds. Medical computer vision: algorithms for big data: international workshop, MCV 2015, held in conjunction with MICCAI 2015, Munich, Germany, October 9, 2015, Revised Selected Papers, Cham. Springer International Publishing; 2016:47–56.
40. van Ginneken B, Tan A, Murphy K, et al. Automated detection of nodules attached to the pleural and mediastinal surface in low-dose CT scans. 2008; 69150X-X-10.
41. Joskowicz L, Cohen D, Caplan N, et al. Inter-observer variability of manual contour delineation of structures in CT. Eur Radiol 2019; 29:1391–1399.
42. Li Q, Liang Y, Huang Q, et al. Volumetry of low-contrast liver lesions with CT: investigation of estimation uncertainties in a phantom study. Med Phys 2016; 43:6608.
43. Deshpande KK, Summers RM, Van Uitert RL, et al. Quality assessment for CT colonography: validation of automated measurement of colonic distention and residual fluid. AJR Am J Roentgenol 2007; 189:1457–1463.
44. Van Uitert RL, Summers RM, White JM, et al. Temporal and multi-institutional quality assessment of CT colonography. AJR Am J Roentgenol 2008; 191:1503–1508.
45. Uppot RN, Sahani DV, Hahn PF, et al. Impact of obesity on medical imaging and image-guided intervention. AJR Am J Roentgenol 2007; 188:433–440.